Romanian Reports in Physics, Vol. 66, No. 4, P. 983–992, 2014

CONDENSED MATTER

SPIN TRANSPORT IN GRAPHENE-BORON NITRIDE HYBRID MATERIALS WITH TRANSITIONAL METAL IMPURITIES

CAMELIA VISAN

"Horia Hulubei" National Institute for Physics and Nuclear Engineering (IFIN-HH), Department of Computational Physics and Information Technologies, 077125 Magurele-Ilfov, Romania, E-mail: cmvisan@nipne.ro

Received October 10, 2013

Abstract. Spin transport in grapheme-boron nitride nanoribbons with transitional metal impurities was investigated in the framework of density functional theory calculations. Several structures with substitutional magnetic impurities on boron and nitrogen are investigated. Following relaxations, the formation energies are calculated. The ballistic spin currents are obtained using non-equilibrium Green's functions formalism and the spin current polarization is extracted. Relatively high spin current polarizations, as well as pronounced spin current switching behaviors are obtained, depending on the type of the transitional metal impurity. Spin density maps confirm the two types of spin transfer characteristics.

Key words: graphene, boron-nitride, formation energy, spin filter, spin current switch.

1. INTRODUCTION

Efficient spin filters are highly important for the future spintronic devices. New developments indicate the possibility of using diluted magnetic semiconductors [1–3] as spin injectors. One example of this type is the hexagonal boron nitride (hBN) monolayer, doped with transitional metal impurities [4, 5]. This is an isomorph of graphene [6–9], with a very similar lattice constant, but rather different electrical properties [10].

Boron nitride is a material from the III-V group with a wide band gap and high chemical stability. The bulk material presents three crystalline forms, namely hexagonal (graphite-like), cubic (sphalerite) and wurtzite. Hexagonal BN has a honeycomb appearence obtained by alternating boron and nitrogen atoms. These are bound in hexagonal layers by strong covalent bonds, while the layers are beeing hold together by weak van der Waals forces. The hBN monolayer is also a promising dielectric, in contrast to graphene, which is a zero-bandgap semiconductor.

Hybrid graphene-hBN materials have been synthesized [11, 12], combining the properties of the large bandgap-hBN semiconductor with conductive properties of graphene. In-plane heterostructures using graphene and hBN have been recently

produced [13]. The shapes of the two domains were controlled using lithography pattering and sequential CVD growth steps. Hybrid structures of this kind, with a single atomic layer, can provide the building blocks for the next generation of flexible two-dimensional electronic and opto-electronic devices. Furthermore a number of applications have been developed, such as field effect transistors [14, 15], atomically thin circuitry [16], resonant tunneling diodes [17], pressure sensors [18], applications using transport gap engineering [19] and other tunneling devices [20].

The two-dimensional BNC monolayer may be truncated to obtain narrow nanoribbons. As contact electrodes, the zigzag graphene nanoribbon [21, 22] (zGNR) is used, which is always metallic. This is in contrast with the zigzag counterpart, where a gap developes when the width of the nanoribbon is decreased. Due to the very small mismatch between the zigzag BN nanoribbon (zBNNR) segment and the zGNR, a natural coupling is ensured. The spin transport has been investigated in this setup, with manganese impurities substitutional on boron [23, 24]. A very recent study investigates spin filtering and magneto-resistive effects at graphene/hBN interface using *ab initio* calculations [25].

In contrast to the bulk systems, here the spin transport is largely influenced by the edge states. Similar features are found in other quasi-one dimensional magnetic nanostructures made of group-III nitrides, such as nanowires with transitional metal impurities (TM), where the surface states have a large impact on the spin current polarization [26–31]. These quasi one-dimensional devices based on III-V semiconductors with transitional metal impurities indicate rather good spin-filter properties and characteristic spin switching behavior.

In this paper the spin transport is investigated in BN nanoribbons connected to metallic graphene electrodes, which contain different TM impurities (Co, Cr, Mn, Fe, Ni), substitutional on either boron or nitrogen. A comparative analysis of the spin transfer characteristics for different types of magnetic impurities is performed, pointing out two types of behaviors – spin filter and spin current switch. Some of the samples indicate features specific to resonant tunneling such as negative differential conductivity.

2. METHOD

The pristine structure is a nanoribbon with a double graphene-hBN heterojunction as described in Ref. [22]. The BN segment consists of 8 boron and 8 nitrogen atoms, while the graphene electrodes are semi-infinite with the same cross-section. The zigzag configuration was chosen since the zGNR is always metallic even for very narrow widths, which is not the case in the armchair configuration. The edges are hydrogen passivated.

Next, transitional metal impurities are introduced at the locations indicated in Fig. 1. Structural relaxations are performed in the DFT framework, using SIESTA code [32, 33], which uses an efficient set of numerical atomic orbitals. The

localized basis set allows linear scaling of the computational time with the size of the system. The structures are relaxed until all forces are less than 0.04eV/Å. The maximum displacement during the relaxation was 0.1Å. The exchange-correlation functional used is the one proposed by Ceperley and Alder in the local spin density approximation. A Monkhorst-Pack scheme with $1 \times 1 \times 10$ mesh points was used for sampling the Brillouin zone.

The initial out of the plane displacement of the TM impurities is followed by a local deformation of the lattice. The resulting bonding lengths are presented in the Table 1. One can see that there is a general trend of decreasing bonding length with increasing the atomic number. An exception is Mn impurity which has larger bonds than Cr and Fe, for both types of substitutions. The Ni impurity substituted on nitrogen indicates also a slightly larger bonding length. Note that the magnetic impurity has three nitrogen first order neighbors, when substituted on boron and three boron neighbors for the nitrogen substitution as one can see from Fig. 1.

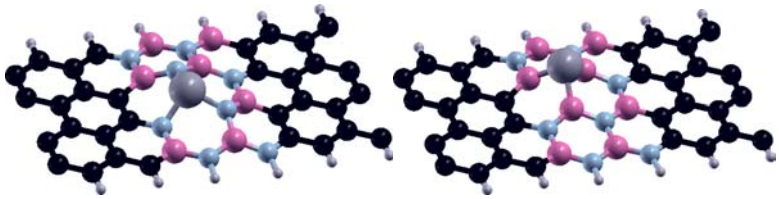

(a) (b)

Fig. 1 – Simulation model structures consisting of graphene electrodes and hBN segment with one Co impurity subtitutional on boron (a) and nitrogen (b).

Table 1

Bonding lengths (averaged over the nearest neighbor) between the transitional metal impurity substituted on boron or nitrogen and the nearest neighbor, *i.e.* nitrogen and boron, respectively. The values are given in Å

	Cr	**Mn**	**Fe**	**Co**	**Ni**
B	1.88	1.95	1.84	1.80	1.79
N	2.44	2.64	2.09	1.81	1.83

Table 2

Formation energies for the structures with TM impurities substituted on boron and nitrogen. The values are given in eV

	Cr	**Mn**	**Fe**	**Co**	**Ni**
B	1.06	2.02	3.49	4.71	5.59
N	3.81	5.35	7.37	7.32	6.78

The formation energies of the point-like defects can be calculated from the following relation:

$$E_f = E_s^{tot} - E_{BNC}^{tot} - n_B \mu_B - n_N \mu_N - n_X \mu_X , \quad (1)$$

where E_s^{tot} is the total energy of the structure with one TM impurity, E_{BNC}^{tot} is the total energy of the pristine BNC structure, $n_{B,N,X}$ are the numbers of particles exchanged with the reservoirs and $\mu_{B,N,X}$ are the chemical potentials of B, N and the TM impurity X (Cr, Mn, Fe, Co, Ni). The chemical potentials are calculated from the alpha phase of boron, molecular N_2 and bcc-Cr, bcc-Fe, fcc-Ni bulk systems. The formation energies for the two types of substitutions are given in Table 2. The general trend observed for boron substitutions is an increase in the formation energy as the atomic number is getting larger. For the nitrogen substitutions, the maximum E_f is reached for the Fe impurity. The structures with nitrogen substitutions have larger formation energies, which is in agreement with the calculations performed on an infinite two dimensional BN lattice with Mn impurities [5]. In the present study, the finite width of the nanoribbon together with the presence of graphene electrodes leads to smaller formation energies, compared to the infinite two dimensional system.

The magnetic moments of the magnetic impurities were set to up–spin configuration during the spin constrained DFT calculations.

The spin transport is analyzed using the Green's functions formalism, implemented in TRANSIESTA [34]. The ballistic transmission functions provide the current for each spin state:

$$I_{\uparrow/\downarrow} = \frac{e}{h}\int \mathrm{d}E T_{\uparrow/\downarrow}(E)\left[f_L\left(E-\mu_L\right)-f_R\left(E-\mu_R\right)\right], \tag{2}$$

where $T_{\uparrow/\downarrow}$ is the spin dependent transmission function, $f_{L/R}$ and $\mu_{L/R}$ are the occupation functions and chemical potentials, respectively. In the limit of low temperatures considered here, the integral defined in Eq. (2) is evaluated on the range $[\mu_L, \mu_R]$ and the occupation functions $f_{L/R}$ are assumed to be step functions. The total transmission function $T = T_\uparrow + T_\downarrow$ is found from:

$$T(E) = Tr[\Gamma_L G^r \Gamma_R G^a], \tag{3}$$

where $G^{r/a}$ are the retarded/advanced Green's functions, while the couplings between the active region and the contacts are accounted by the self-energies $\Gamma_{L/R}$.

One can define a spin current polarization at a certain bias as the ratio between the spin current difference and the total current:

$$P_I = \frac{I_\uparrow - I_\downarrow}{I_\uparrow + I_\downarrow}. \tag{4}$$

This quantity is important in establishing the quality of a spin filter or a spin current switching device. For the former, one needs high values for the absolute

value for the spin current polarization, ideally $|P_I| = 1$, while for the latter, a rapid change in the spin current polarization dP_I/dU is sought.

3. RESULTS

The spin dependent transmission functions for structures with TM impurities substitutional on boron and nitrogen are depicted in Figs. 3 and 4, respectively. The data is obtained for zero bias and is relevant for the linear (small bias) regime. One can define a transmission polarization coefficient in a similar way as in Eq. (4),

$$P_T = \frac{T_\uparrow - T_\downarrow}{T_\uparrow + T_\downarrow}.$$

As indicated in Table 3, for the systems with TM impurities substituted on boron, one finds relatively large up-spin polarization for Cr and Mn, a large down-spin polarization for Co and quite small values for Fe and Ni. For the substitutions on nitrogen, one observes very small values for P_T in the case of Mn, Co and Ni, while for Cr and Fe average polarizations for the down-spin and up-spin are found, respectively. These values for the transmission polarization coefficient can be correlated with the spin current polarization, which are discussed later.

Table 3

The transmission polarization coefficient at Fermi energy, for U=0 V

	Cr	**Mn**	**Fe**	**Co**	**Ni**
B	0.76	0.85	0.20	-0.89	-0.14
N	-0.22	0.04	0.29	0.01	0.12

The spin transfer characteristics are next investigated for each impurity type and for both boron and nitrogen substitutions as a function of applied bias.

The pristine BN nanoribbon system with graphene electrodes is poorly conductive, due to the large bandgap of the semiconducting segment. The role of hBN is evidenced as several gaps appear in the density of states of the ideal graphene nanoribbon [20]. These gaps tend to close once a transitional metal impurity, such as Mn, is introduced.

Figures 5 and 6 show the spin resolved currents for the two types of substitutions. A typical feature observed in resonant transport is the negative differential conductivity. This was also found here, in systems with Cr and Ni substituted on boron and for all systems with substitutions on nitrogen, except Co. The presence of TM impurities also produces an enhancement in conduction, compared with the pristine graphene-hBN-graphene nanoribbon. Larger currents are observed for samples with Cr, Co substituted on boron and for the samples with Mn, Ni substituted on nitrogen. More important is however the spin separation which occurs in the presence of the TM impurities.

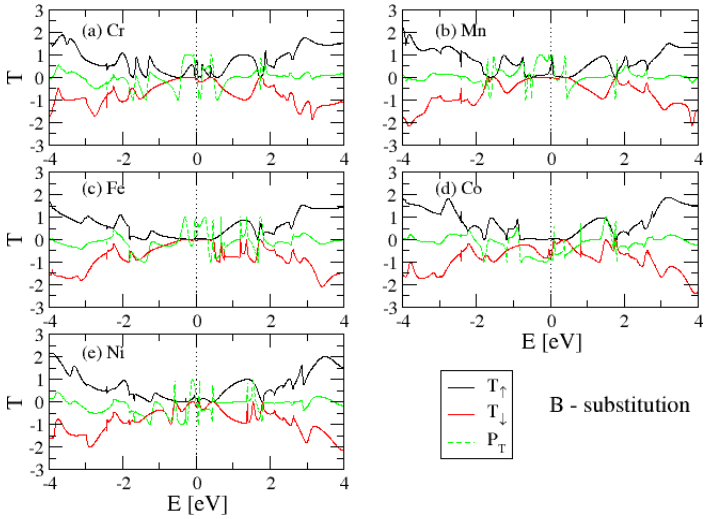

Fig. 3 – Spin dependent transmission functions for structures with TM substitutions on *boron*: $T_{\uparrow}$ (black/positive), $-T_{\downarrow}$ (red/negative) and the transmission polarization coefficient (green/dashed).

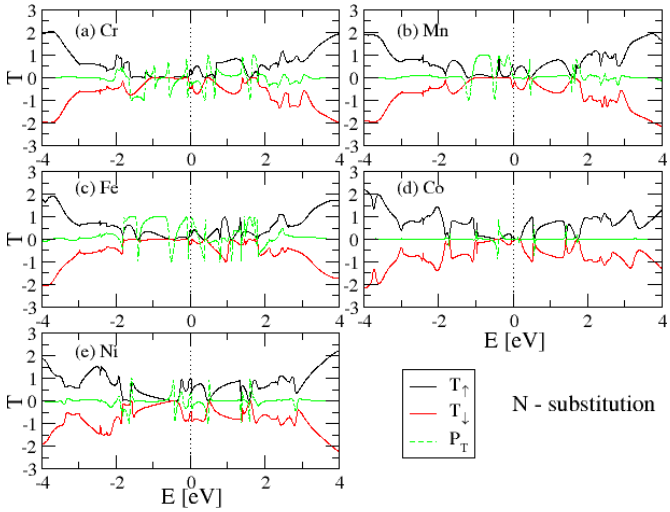

Fig. 4 – Spin dependent transmission functions for structures with TM substitutions on *nitrogen*: $T_{\uparrow}$ (black/positive), $-T_{\downarrow}$ (red/negative) and the transmission polarization coefficient (green/dashed).

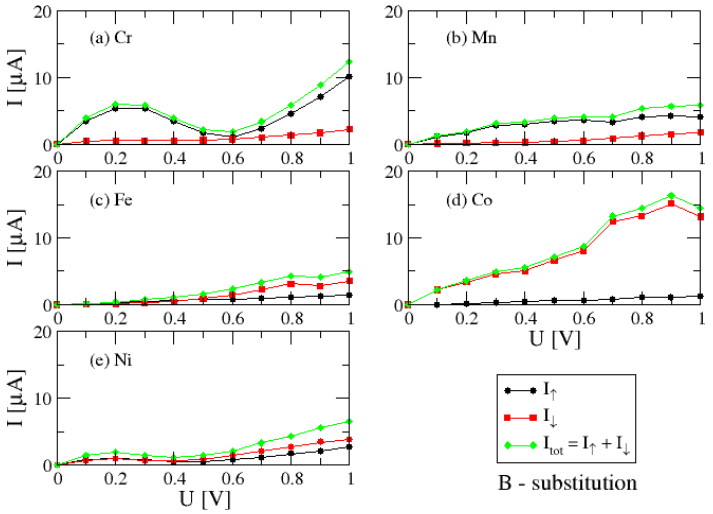

Fig. 5 – Spin currents for systems with transitional metal impurities (Cr, Mn, Fe, Co, Ni) substituted on *boron*: $I_\uparrow$ (circles/black), $I_\downarrow$ (squares/red), total current (diamonds/green).

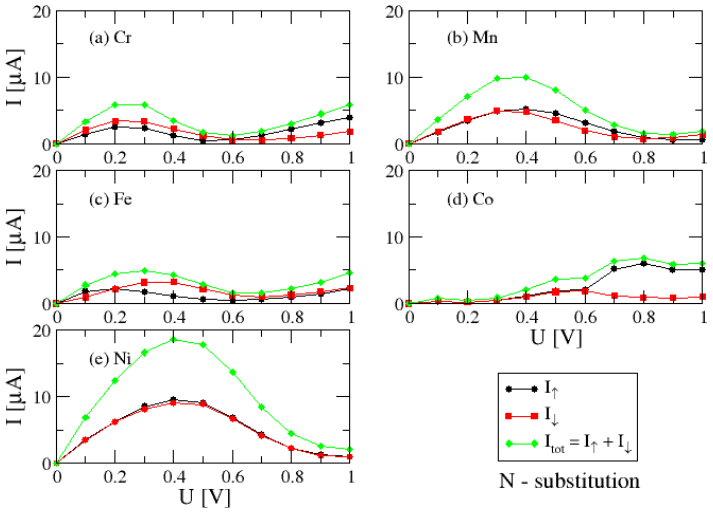

Fig. 6 – Spin currents for systems with transitional metal impurities (Cr, Mn, Fe, Co, Ni) substituted on *nitrogen*: $I_\uparrow$ (circles/black), $I_\downarrow$ (squares/red), total current (diamonds/green).

Using the data presented in Figs. 5 and 6 one can calculate the spin current polarization, according to Eq. (4), as a function of applied bias. The results are indicated in Fig. 7. First of all, one can see a gradual change in the spin current polarization for the different TM impurities in increasing atomic number. As it was mentioned in the previous section, two types of spin transfer characteristics may be found, namely of spin-filter and spin current switch. In the former category are

found the systems with Mn and Co substituted on boron, while in the latter one may include samples with Co substituted on nitrogen and Ni on boron.

The sample containing Co substitutions offers an noteworthy example for the two types of spintronic behaviors. The spin-filtering effect is rather robust with high values (>80%) on the entire bias range. This values are larger than in other group-III nitrides quasi-one dimensional systems with TM impurities [26, 27]. On the other hand the spin switching behavior is also very pronounced as the polarization has a rather sharp increase at 0.65V.

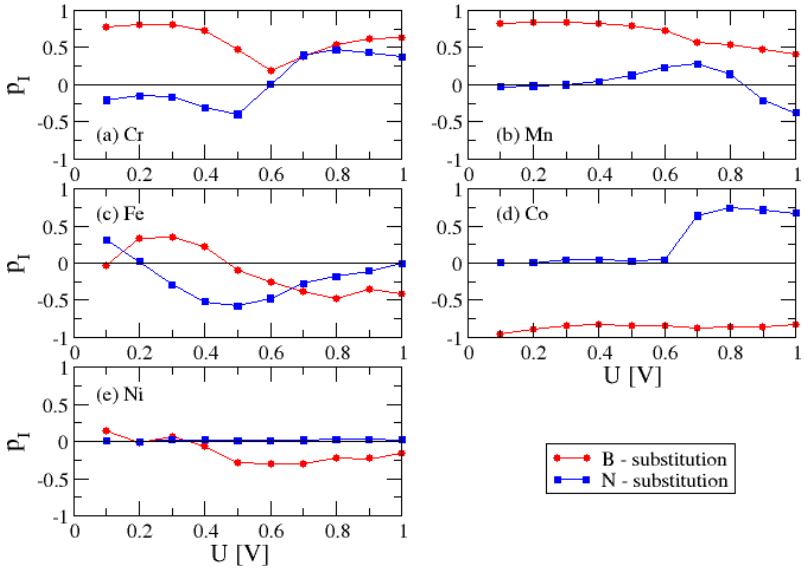

Fig. 7 – Spin current polarization for systems with transitional metal impurities (Cr, Mn, Fe, Co, Ni) substituted on boron (circles/red) or nitrogen (squares/blue).

The spin densities are represented in Fig. 8 in order of further investigate this rather different behaviors in the spin transfer characteristics obtained in the structures with Co substitutions. One can see that in the case of boron substitution the spin density located around the Co impurity is significant at both low and high bias. Therefore the two spin states are scattered differently and, as a result, the large spin current polarization is achieved. By contrast, in the case of the nitrogen substitution, there is a large difference in the spin density located at the impurity site for the two biases. At small bias, the absence of the spin polarization on the Co impurity results in a lack of spin separation. However at large bias, the spin density becomes comparable with the one corresponding to boron substitution and the spin current polarization increases significantly. The structure therefore behaves a spin current switch. One should also note the higher polarization of the edge atoms, which play the most important role in the spin transport [17].

(a) Boron substitution:

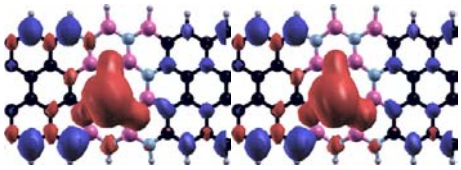

U=0.1V U=1.0V

(b) Nitrogen substitution:

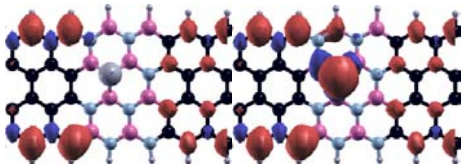

U=0.1V U=1.0V

Fig. 8 – Spin density for the structure with Co impurity substituted on boron (a) and nitrogen (b), at low bias (U=0.1V) and at high bias (U=1.0V).

4. CONCLUSIONS

The spin transport properties were investigated in boron nitride nanoribbons with transitional metal impurities (Co, Cr, Mn, Fe, Ni), connected to graphene electrodes.

Performing contrained spin DFT calculations, the structures are relaxed and the formation energies of the point-like defects are extracted. These provide information about stability of different structures, depending on the type of substitution, *i.e.* boron or nitrogen.

The spin resolved currents are obtained, revealing negative differential conductance for many of the samples, especially those with substitutions on nitrogen. Introducing the transitional metal impurities, the conductance is also increased, compared with the pristine system.

The spin current polarization is obtained and two types of spin transfer characteristics are pointed out: spin filtering and spin switching effects. Belonging to the former class are systems with nearly constant and high values of spin current polarizations, such as the systems with Mn and Co substituted on boron. The values are larger than in other quasi one-dimensional TM-doped systems, made of group-III nitrides. The latter class of spintronic devices corresponds to a significant and sharp increase in the spin current polarization and is represented by the samples with Co substituted on nitrogen and Ni substituted on boron.

The systems with Co substitutions are further analyzed in detail. The spin density analysis explains the different behavior for the two types of substitutions, at low and high biases.

To conclude, the comparative analysis performed on graphene-hBN systems with different transitional metal impurities indicates the structures are promising candidates for future spintronic devices, either as efficient spin injectors or as spin commutators.

Acknowledgements. Discussions with G. A. Nemnes are gratefully appreciated. This work was supported by the Romanian National Authority for Scientific Research, under grant PN 09370104/2013.

REFERENCES

1. T. Dietl, H. Ohno, F. Matsukura, J. Cibert, D. Ferrand, Science, **287**, 1019 (2000).
2. H. Ohno, F. Matsukura, Solid State Commun., **179**, 117 (2001).
3. M. Negoita, E.A. Patroi, C.V. Onica, Rom. Rep. Phys., **62**, 115 (2010).
4. D. Ma, Z. Lu, W. Ju, and Y. Tang, Journal of Phys. Condensed Matter, **24**, 145501 (2012).
5. T.L. Mitran, A. Nicolaev, G.A. Nemnes, L. Ion, and S. Antohe, Journal of Phys. Condensed Matter, **24**, 326003 (2012).
6. M. Dragoman, Rom. Rep. Phys. **65**, 792 (2013).
7. M. Dragoman, Proceedings of the Romanian Academy – Series A, **10**, 91 (2009).
8. V. Damljanovic, R. Kostic, R. Gajic, Rom. Rep. Phys., **65**, 193 (2013).
9. V. Damljanovic, R. Gajic, Phys. Scr., **T149**, 014067 (2012).
10. R. Strana, I. Casian-Botez, R. Litoiu, A. Aluculesei, I. Ionita, I. Gottlieb, Rom. J. Phys., **55**, 1111 (2010).
11. Li Song, Lijie Ci, H. Lu *et al*., Nano Letters, **10**, 3209 (2010).
12. Lijie Ci, Li Song, C. Jin *et al*., Nature Materials, **9**, 430 (2010).
13. Zheng Liu, Lulu Ma, Gang Shi, Wu Zhou *et al.*, Nature Nanotechnology, **8**, 119 (2013).
14. L. Britnell, R.V. Gorbachev, A.K. Geim, L.A. Ponomarenko, A. Mishchenko, M.T. Greenaway, T.M. Fromhold, K.S. Novoselov& L. Eaves, Nature Communications, **4**, 1794 (2013).
15. H. Wang *et al.,* IEEE Elec. Dev. Lett., **32**, 1209 (2011).
16. M.P. Levendorf *et al.,* Nature, **488**, 627 (2012).
17. V. Hung Nguyen, F. Mazzamuto, A. Bournel, P. Dollfus, J. Phys. D Appl.Phys., **45**, 325104 (2012).
18. Y. Xu *et al.,* Appl. Phys. Lett., **99**, 133109 (2011).
19. A. Lopez-Bezanilla, S. Roche, Phys. Rev., B **86**, 165420 (2012).
20. L. Britnell *et al.,* Nano Lett., **12**, 1707 (2012).
21. V. Barone, O. Hod, and G.E. Scuseria, Nano Letters, **6**, 2748 (2006).
22. Young-Woo Son, L. C. Marvin , G. L. Steven, Nature, **444**, 347 (2006).
23. G.A. Nemnes, J. Nanomater., **2012**, 748639 (2012).
24. G.A. Nemnes and S. Antohe, Materials Science and Engineering, B **178**, 1347 (2013)
25. Simon Mutien-Marie Dubois, Xavier Declerck, J.-C. Charlier, and Michael C. Payne, ACS Nano, **7**, 4578 (2013).
26. Y. Yang, Q. Zhao, X.Z. Zhang *et al*., Appl. Phys. Lett., **90**, 092118 (2007)
27. P. Dev, H. Zeng and P. Zhang, Phys. Rev., B **82**, 165319 (2010).
28. Hyun Kum *et al*, Appl. Phys. Lett., **100**, 182407 (2012).
29. H. Li, H. Q. Bao, B. Song *et al.,* Physica, B **403**, 4096 (2008).
30. G. A. Nemnes, J. Nanomater., **2013**, 408475 (2013).
31. G. A. Nemnes, C. Visan, EPJ Plus, **128**, 131 (2013).
32. J.M. Soler, E. Artacho, J.D. Gale, A. Garca, J. Junquera, P. Ordejon, D. Sanchez- Portal, J. Phys., Cond. Mater. **14**, 2745 (2002).
33. P. Ordejon, E. Artacho, J.M. Soler, Phys. Rev., B **53**, R10441(1995).
34. M. Brandbyge, J.-L. Mozos, P. Ordejon, J. Taylor and K. Stokbro, Phys. Rev., B **65**, 165401 (2002).